STUDY ON THE VARIATION LAW OF LAYERED STRESSES OF OVERHEAD CONDUCTORS IN HIGH-ALTITUDE COLD ZONE

Zhilei HAN[a], Yongdou LIU[a,b*], Hongwei ZhANG[a], Jiali DUAN[a], Zhidong CHEN[a,b]

[a]School of Civil Engineering and Hydraulic Engineering, Qinghai University, Xining, Qinghai, China;

[b]Qinghai Provincial Key Laboratory of Energy-Saving Building Materials and Engineering Safety, Xining, China

Yongdou LIU; E-mail: liu_yongdou@qhu.edu.cn

Abstract*: A numerical method is proposed for solving the layered stresses of overhead conductors and applied to analyze the stress distribution of the LGJ-400/35 operating in high-altitude cold zone climatic conditions. The method is crucial for achieving a dynamic increase in line current, ensuring strength and sag safety during periods of peak power demand, and preventing strand breakage caused by fatigue under long-term service conditions. Based on the temperature field results, the layered stress of the conductor is determined through internal and external force balance and deformation compatibility. The method fully considers the transversal deformation of the strands caused by interlayer extrusion, Poisson's effect, and temperature changes.*

Keywords*: Finite element method; Layered stress; Overhead conductors; Thermo-stress field; Transversal deformation;*

1. Introduction

With the rapid development of economy and surge of electricity consumption, the existing power grid is facing challenges in meeting the transmission requirements during peak periods of power usage. To address this issue, in addition to constructing new lines, it may be more economic to dynamically increase the carrying current of the grids to fully exploit the potential of the existing grids. In this case, it is imperative to precisely analyze the stress characteristics of overhead conductors. The climate changes (including wind speed, solar irradiance condition, and environmental temperature), especially those in high-altitude cold zone, can affect the temperature distribution in the overhead conductors remarkably and further influences the stress field and sag of overhead conductor [1]. Large sags lead to insufficient distance from the ground. Therefore, it is important to propose a numerical method for solving the layered stresses of overhead conductors under operating conditions based on fully considering the climatic conditions.

When solving the stress field of the conductor, the traditional methods assume that the temperature distribution inside the conductor is uniform. [2-4] The radial temperature of the conductor, however, is not uniformly distributed, and its radial temperature difference can

reach 5~15℃[5]. Additionally, experimental studies have measured the radial temperature distribution of energized overhead conductors both indoors [6, 7] and outdoors [8, 9], revealing that the temperature difference within the conductor's cross-section is significant and cannot be neglected. The effects of wind speed, wind direction, ambient temperature, and solar irradiance on the temperature distribution of the overhead and layered stress were analyzed by Bena *et al.* [10]. Lin *et al.* [11] developed a finite element model to simulate the layered stress distribution of conductors after being subjected to tension during operation. The equivalent stress distribution of the steel core aluminum stranded conductors was analyzed under conditions of considering relative slip between the strands [12]. Morgan analyzed the tensile strength of overhead conductors under high-temperature conditions. [13] Rawlins *et al.* studied the internal damping of tensive cables during flexure by transverse vibration. [14]

According to previous studies, the temperature distribution of overhead conductors is significantly affected by operating conditions, which will further influence their layered stress. Therefore, it is necessary to fully consider the effects of radial temperature field when solving the layered stress of overhead conductors. The numerical method for systematically solving the temperature and layered stress of overhead conductors is very important to prevent fatigue problems. This paper presents a systematical numerical method for solving the layered stresses depending on the accurate temperature distribution of overhead conductors. These numerical methods are established based on the deformation compatibility of strands, material constitutive behavior and internal and external force balance function of overhead conductors. The systematical numerical method fully considered the winding structure, interlayer extrusion, Poisson effect and transverse and longitudinal deformation of the strand. The proposed systematical numerical method is applied to the calculation of layered stresses of the steel core aluminum conductor LGJ-400/35. Based on the results, this study analyzed the effects of current carrying capacity, convection condition and ambient temperature on the layered stresses of overhead conductor.

2. The principle of thermo field calculation

2.1. Two-dimensional steady-state thermal equilibrium equation

The heat exchange occurring among the strands of an overhead conductor and between a strand and its surrounding air can be mathematically described using a two-dimensional steady-state heat conduction equation [4]. The thermal equilibrium equation for the conductor within its complete cross-sectional area Ω can be formulated as follows:

$$\lambda div(\mathbf{grad}T) + s = 0, (x, y) \in \Omega \tag{1}$$

The heat dissipation balance equation on the boundary Γ of cross-sectional area Ω [15] is

$$q_n = -\lambda \mathbf{grad}T \cdot \mathbf{n} = \alpha(T_s - T_a), (x, y) \in \Gamma \tag{2}$$

For two-dimensional problems, the components of the temperature gradient $\mathbf{grad}T$ are denoted as $\partial T / \partial x$ and $\partial T / \partial y$, representing the first derivatives of the conductor's

temperature field T with respect to coordinates x and y respectively. The term "div" represents the divergence of a vector; λ denotes the isotropic thermal conductivity of steel core, aluminum strands or air. The variable s refers to the heating rate per unit volume within the conductor's steel core or aluminum strands [16], which have different values in each material. The term q_n denotes the rate of heat dissipation in the direction normal to the surface of the conductor, where $\mathbf{n}$ represents the normal direction with components n_x and n_y; α is the composite coefficient of heat dissipation; T_s and T_a refer to surface (or boundary) temperature and ambient temperature, respectively.

By employing the principle of virtual work, equation (1) is integrated by means of integration by parts, and then the boundary condition specified in equation (2) are introduced to derive the following weak form of steady-state heat balance equation.

$$\int_{\Omega} grad(\delta T)\cdot grad(T)\lambda d\Omega + \int_{\Gamma} \delta T\alpha T d\Gamma = \int_{\Gamma} \delta T\alpha T_a d\Gamma + \int_{\Omega} \delta T s d\Omega \tag{3}$$

A finite element computing program (Fortran) for solving the two-dimensional steady state nonlinear temperature field problem can be generated by writing all the integral terms in the above equation into FEPG [17] language according to the grammar rules of the finite element language generation system. Based on the generated program, numerical modeling, finite element mesh division and finite element solution can be carried out for this kind of problems. The computational program developed by the authors has undergone mesh convergence testing and has been compared with experimental results [18].

2.2. Numerical process for calculating thermo field of the overhead conductors

To fully account for the effects of voids and internal structure on the thermal conduction across the cross-section of overhead conductors, we modeled the steel core, aluminum strands, and air in detail. Each component was meshed using triangular elements, as shown in fig. 1. The heating rate per unit volume within the conductor's steel core or aluminum strands (represented by s_s and s_a respectively) and the composite coefficient of heat dissipation[16] α are key to solving weak form of steady-state heat balance equation (i.e., Eq. (3)) of overhead conductors. The heating rate per unit volume within the conductor's steel core or aluminum strands are related to the average temperature of cross section T_{av} and surface (or boundary) temperature T_s of the overhead conductors which can only be obtained upon the solution of the thermal field. Therefore, an initial temperature field needs to be set firstly in order to carry out the solving process. Then, the real solution of the radial temperature field can be obtained after several iterations. The fixed-point iteration method is adopted herein, and the numerical process for calculating thermo field of the overhead conductors is illustrated in fig. 2.

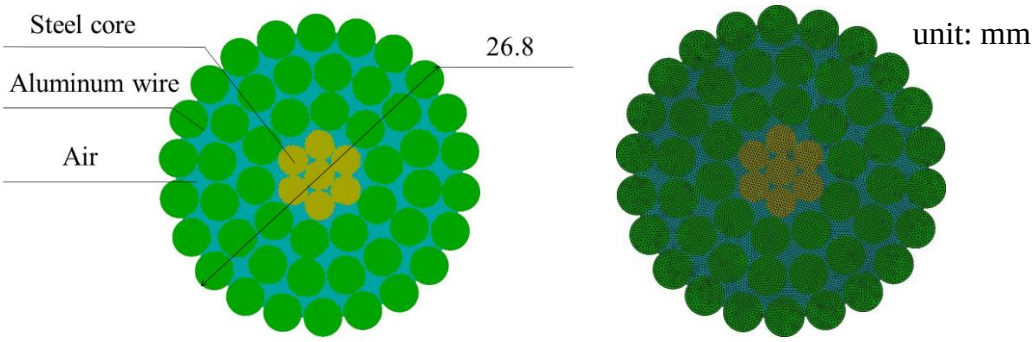

Figure 1.Cross-sectional dimensions and mesh division of LGJ-400/35 steel core aluminum stranded wire.

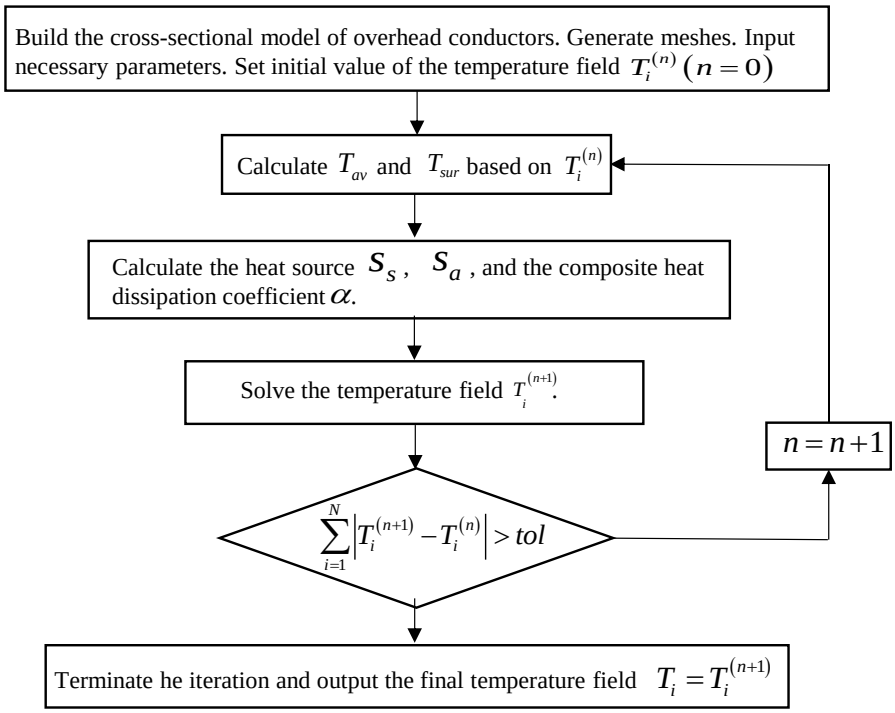

Figure 2. Calculation Flowchart

Note: *N* represents the number of degrees of freedom in the finite element model; $T_i^{(n)}$ and $T_i^{(n+1)}$ represent the temperature values at node *i* for the n^{th} and $(n+1)^{th}$ iteration steps, respectively; *tol* is the tolerance of calculation. According to the above process, the parameters required to solve the steady-state heat balance equation (i.e., Eq. (3)) are: (1) current, in unit A; (2) resistance, in unit Ω; (3) steel core resistivity, in unit $\Omega\cdot\mathrm{m}$; (4) aluminum conductor resistivity, in unit $\Omega\cdot\mathrm{m}$; (5) total cross-sectional area of the steel core, in unit m^2; (6) total cross-sectional area of the aluminum conductor, in unit m^2; (7) wind speed, in unit m/s; (8) wind direction, in unit °; (9) ambient temperature, in unit ℃; (10) altitude, in unit m; (11) solar irradiance, in unit $\mathrm{W/m^2}$.

3. Layered stresses of overhead conductors

To solve the layered stresses of strands, three essential relationships are required [17], they are deformation compatibility condition, constitutive relationship of material, and

resisting and external force equilibrium. The present study assumes that both the steel core and aluminum strand exhibit linear elastic behavior, thus obviating the need for further elaboration on their constitutive relationship [19].

3.1. Deformation compatibility condition

A straight strand wire with length S_i can be obtained by unfolding a full circle of strand wire AB in the i^{th} layer which has a longitudinal length of L_{s_i} as shown in fig. 3. The twisted wire is R_i away from the centroid of the conductor cross-section O. The projected length of the unfolded wire on the cross section is $R_i\varphi_i$. Assuming that there is longitudinal tensile strain ε_0 present in the conductor, then it will undergo displacement in both its longitudinal direction $\varepsilon_0 L_{s_i}$ and transverse inward direction ΔR_i. Correspondingly, it can be observed that the unfolded wire is displaced vertically by $\varepsilon_0 L_{s_i}$ and horizontally by $\varphi_i \Delta R_i$, that is, from its original configuration AB to AB". Based on the geometric relationship of the unfolded wire, it is observed that BC+CB"=BB", that is [20,21],

$$\varepsilon_0 L_{s_i} = \Delta S_i / \sin\alpha_i + \Delta R_i \varphi_i / \tan\alpha_i \tag{4}$$

In this equation, the term α_i is the twisted angle of the i^{th} layer of strand wire, it represents the angle between the tangential direction of the i^{th} layer strand wire and the cross-section of the overhead conductor. The variable φ_i represents the ratio between the distance of the i^{th} layer of twisted wire to the centroid of the conductor cross-section O and the projected length of the unfolded wire on the cross section, that is,

$$\varphi_i = S_i \cos\alpha_i / R_i \tag{5}$$

The geometric relationship of the unfolded wire shows that

$$\sin\alpha_i = L / S_i \tag{6}$$

Then, the tensile strain of every wire in the i^{th} layer of strand can be expressed by

$$\varepsilon_i = \Delta S_i / S_i \tag{7}$$

By dividing S_i on both sides of the Eq. (4) and then introducing Eq. (5)~ Eq. (7) into Eq. (4), we can establish the relationship between tensile strain for the strand wire in the i^{th} layer ε_i and the longitudinal strain ε_0 of the conductor, as follows:

$$\varepsilon_i = \varepsilon_0 \sin^2\alpha_i - (\Delta R_i / R_i)\cos^2\alpha_i \tag{8}$$

The transverse displacement of the i^{th} layer strands ΔR_i consists of three parts [22]: 1) the displacement of the strand wire caused by Poisson effect when it is stretched along its own axis, 2) the displacement resulting from the mutual compression between layers, and 3) transverse displacement induced by temperature changes.

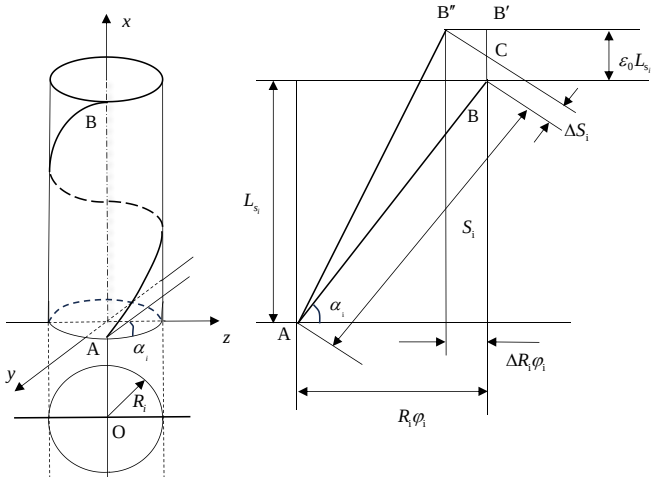

Figure 3. Unfolding diagram of the i[th] twisted strand

3.2. Resisting and external force equilibrium

An equilibrium equation can be established at every location of a span by considering the resistance contributed by all the strand wires and the external force which can be obtained analytically. The calculation of the resisting and external forces will be elaborated below.

The resisting force of the entire cross section of the overhead conductor can be determined by summing up the longitudinal projection of the axial force acting on each individual strand wire, i.e.,

$$p(\varepsilon_0) = \sum_{i=1}^{n} p_i n_i \sin\alpha_i \tag{9}$$

Where n_i indicates total amount of the strand wires in the i^{th} layer.

The axial force of a single wire in i^{th} layer can be determined based on the assumption of linear elasticity and the consideration of temperature strain, i.e.,

$$p_i = E_i(\varepsilon_i - \varepsilon_{iT})A_i \tag{10}$$

In the equation, E_i and A_i represent the modulus of elasticity and cross-sectional area of a single strand wire in the i^{th} layer, respectively.

An overhead conductor is illustrated in fig. 4 with a span length of l and weight per unit length of γ. Its right hanging point B has a relative vertical height of h and a corresponding elevation angle β with respect to the left hanging point A. For a section at a horizontal distance x from the left point A, its external force [23] in the longitudinal direction $N(x)$ can be calculated analytically based on the horizontal tensile stress at the lowest point σ_0.

$$N(x) = \sigma_0 A_0 \sqrt{1 + \left[\tan\beta - \frac{\gamma(1-2x)}{2\sigma_0 \cos\beta}\right]} \tag{11}$$

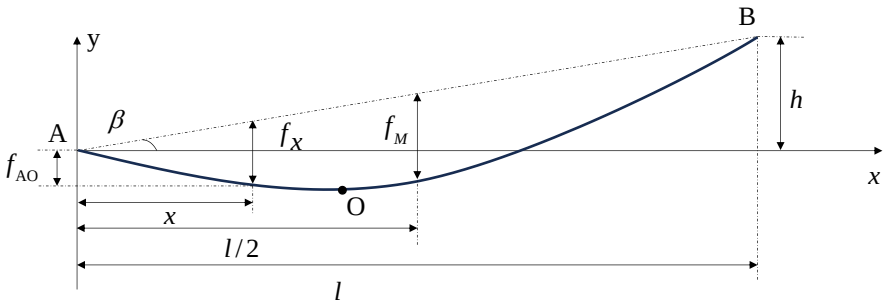

Figure 4. Schematic diagram of overhead conductors

3.3. Numerical process to solve the layered stresses

The temperature field is a function of the layered stress but not vice versa. The thermal field of the cross-section for the overhead conductor is solved separately through the finite element method which is elaborated in section 3. The layered stresses are solved in the following steps by setting the temperature-induced thermal strain is then used as the initial strain:

Step 1: Read in the temperature field, as well as the parameters of very layer of strand wire (including number of the strand wires in i^{th} layer n_i, elastic modulus E_i, Poisson's ratio μ_i, radius of a single strand wire r_i, cross-sectional area of a single strand wire A_i), the distance x of the cross-section to the left hanging point, and the unit linear weight of the overhead conductor γ.

Step 2: Calculate the temperature-induced thermal strain ε_{iT} by using the thermal strain for the j^{th} layer. Assume initial transverse displacement in the i^{th} layer strand wires $\Delta R_i^{(0)}$ to be zero, and estimate the range of axial strains (ε_{01}, ε_{02}) of the overhead conductor. Set the maximum iterative number IterN.

Step 3: solve the equilibrium[22] at position x and obtain axial strain ε_0 of overhead conductor by sub-steps 3.1~3.8, as long as the iteration number i is less than IterN:

3.1 Calculate the resisting forces $p(\varepsilon_{01})$ and $p(\varepsilon_{02})$ by using the procedure in section 3.2.

3.2 Obtain unbalance forces $f(\varepsilon_{01})$ and $f(\varepsilon_{02})$ by using the resisting and external force equilibrium.

3.3 Compute a new strain boundary point, $\varepsilon = \varepsilon_{02} - f(\varepsilon_{02})(\varepsilon_{02} - \varepsilon_{01}) / (f(\varepsilon_{02}) - f(\varepsilon_{01}))$.

3.4 If $(\varepsilon_{01} - \varepsilon) / \varepsilon_{01} \le \zeta_{tol}$, exit the loop and output the axial strain $\varepsilon_0 = \varepsilon$.

3.5 Calculate the unbalance force $f(\varepsilon)$ at the strain ε, and update iteration number $i = i + 1$.

3.6 If $f(\varepsilon) f(\varepsilon_{02}) < 0$, update the lower strain boundary ε_{01} to be ε_{02} and $f(\varepsilon_{01})$ to be $f(\varepsilon_{02})$.

3.7 update the upper strain boundary $\varepsilon_{02} = \varepsilon$ and $f(\varepsilon_{01}) = f(\varepsilon)$.

3.8 If i > IterN , output iteration failure; otherwise, output the axial strain ε_0, resisting force $P(\varepsilon_0)$, layered stress σ_i (dividing the axial force p_i by the cross-sectional area A_i of the wire), layer strain ε_i and compressive force q_i.

4. Examples

Considering the proposed numerical method has undergone comprehensive validation [24], additional details are not presented herein. This research focuses on overhead conductors, particularly the LGJ-400/35 model of aluminum-clad steel-reinforced aluminum conductors, within the unique climatic challenges of high-altitude cold zone. It explores the dynamics of temperature distribution across layered stress as influenced by current load and climatic conditions. The goal is to furnish theoretical underpinnings for ensuring the reliable operation of overhead transmission lines in these challenging climatic conditions.

4.1. Parameters and model

The LGJ-400/35 aluminum-clad steel-reinforced aluminum conductor features the following electrical parameters: resistivities of the steel core and the aluminum strands are designated as $\rho_{s1} = 20\times10^{-8}(\Omega\cdot\mathrm{m})$ and $\rho_{s2} = 2.8\times10^{-8}(\Omega\cdot\mathrm{m})$ respectively, the conductor's direct current resistance is denoted as $R_{dc} = 0.07389\ \Omega/\mathrm{km}\ (20°C)$. Regarding its thermal characteristics, the thermal conductivity coefficients for the steel core and the aluminum conductors are identified as $k_s = 80\ \mathrm{W/(m\cdot °C)}$ and $k_a = 237\mathrm{W/(m\cdot °C)}$, correspondingly. The thermal conductivity of air within the internal voids of the overhead conductor is denoted by $k_{air} = 2.42\times10^{-2} + 3.6\times10^{-5}(T_{av} + T_a)$, which is a function of both the average temperature of the conductor T_{av} and ambient temperature T_a. The geometric specifications of this overhead conductor model are detailed in tab. 1 [25]. The cross-sectional dimensions of the steel-core aluminum stranded wire LGJ-400/35 are depicted in fig. 1. Triangular elements were utilized for the thermal field analysis, featuring a maximum element size of 0.3 mm. The model comprises a total of 14,768 elements and 7,739 nodes.

Table 1. Geometric specifications of the LGJ-400/35 steel core aluminum stranded wire

Steel ratio /%	Area /mm^2			The number of single wire roots		Single wire diameter /mm		Diameter /mm	
	Al	Steel core	total	Al	Steel	Al	Steel	Steel core	Stranded wire
8.7	391	34.3	425	48	7	3.2	2.5	7.5	26.8

Note: the nominal cross-sectional area of aluminum (aluminum-steel) is 400 (35) mm^2; the rated tensile strength is 103.67kN.

4.2. Impact of climatic conditions on the layered stresses

This section explores the layered stress as influenced by variables such as current load, wind velocity, solar irradiance intensity, ambient temperature, and their interplay.

4.2.1. Wind speed

Wind speed is one of the crucial factors influencing stress fields of conductors. To analyze the variations in the field under different wind speeds, we consider wind speed as a variable. The rated current is set at 580A, with specified values for solar irradiance intensity of $S = 300W/m^2$ and ambient temperature of $T_a = 20°C$, at an elevation of 2250 meters. Data from July 5 to July 7, 2022, was taken from the representative city of Xining

in high-altitude cold zone, with wind speeds recorded (source: http://www.wheata.cn/). According to fig. 5, the maximum and minimum wind speeds on July 5 were 0.161 m/s and 2.35 m/s, respectively; on July 6, they were 0.151 m/s and 1.438 m/s; and on July 7, they were 0.151 m/s and 3.362 m/s, with the range varying from 0.151 m/s to 3.362 m/s. Therefore, a wind speed range of 0.1 m/s to 3.5 m/s was chosen to study the variations in the stress fields of overhead conductors with changes in wind speed.

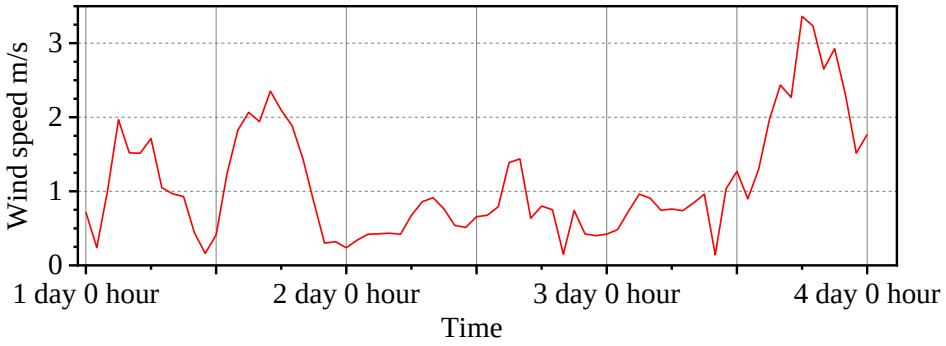

Figure 5. Wind speed schedule for three days from July 5th to 7th, 2022

Figure 8 shows the changes in the layered stresses of the overhead conductor with varying wind speeds. It is observed from the figure that as the wind speed increases from 0.1 m/s to 3.5 m/s, stress in the internal steel core (in the 1st and 2nd layers) decreases from 92.358 MPa to 61.807 MPa (with a fluctuation of 30.551 MPa), and from 91.916 MPa to 61.537 MPa (with a fluctuation of 30.379 MPa), respectively. The stress in the external aluminum strands (in the 3rd, 4th, and 5th layers) changes from 5.626 to 8.465 MPa (with a fluctuation of 2.839 MPa), from 9.709 to 12.375 MPa (with a fluctuation of 2.666 MPa), and from 16.515 to 18.927 MPa (with a fluctuation of 2.412 MPa).

4.2.2. Solar irradiance

Solar irradiance is one of the key factors affecting the stress fields of conductors. To analyze variations in layered stress under different solar irradiance, we consider solar irradiance as a variable while keeping other parameters constant: the rated current 580A, wind speed $v_W = 1\,\mathrm{m/s}$, wind direction angle 90°, forced convection, ambient temperature $T_a = 20°C$, and an elevation of 2250m. Solar irradiance data from July 5 to July 7, 2022, was collected from Xining (a representative city in high-altitude cold zone of China). As shown in fig. 6, the minimum solar irradiance on July 5th, 6th, and 7th were all $S = 0\ \mathrm{W/m^2}$, with the maximum conditions reaching $820.569\ \mathrm{W/m^2}$, $848.036\ \mathrm{W/m^2}$ and $846.293\ \mathrm{W/m^2}$, respectively. Therefore, a solar irradiance range of $0 \sim 800\ \mathrm{W/m^2}$ is used to study the variations in the layered stresses of overhead conductors with changes in solar irradiance.

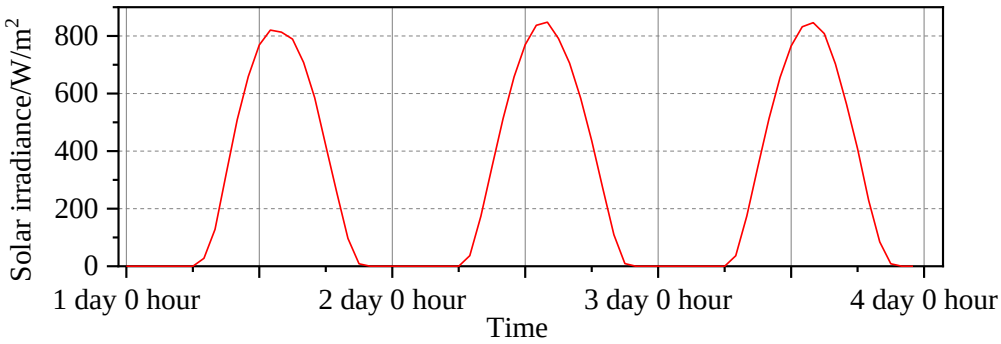

Figure 6. Solar irradiance from July 5th to 7th, 2022

Figure 9 shows the variations in the layered stresses of the overhead conductor with changes in solar irradiance. From the data, it is observed that as solar irradiance increases from $0\,\mathrm{W/m^2}0$ to $800\,\mathrm{W/m^2}$, stresses action on internal steel core (in the 1st and 2nd layers) increases from 68.429 MPa to 74.41 MPa (with a fluctuation of 5.981 MPa), and from 68.119 MPa to 74.073 MPa (with a fluctuation of 5.954 MPa), respectively. The stress in the external aluminum strands (in the 3rd, 4th, and 5th layers) changes from 5.937 to 8.669 MPa (with a fluctuation of 2.732 MPa), from 10.778 to 12.097 MPa (with a fluctuation of 1.319 MPa), and from 17.82 to 18.917 MPa (with a fluctuation of 1.097 MPa). In plateau zone with long sunlight hours and abundant solar irradiance, the impact of solar irradiance on the layered stresses of overhead conductors is not as significant as wind speed but should not be overlooked.

4.2.3. Ambient temperature

Ambient temperature is another critical factor influencing the layered stresses of the overhead conductors. To analyze the changes in the layered stresses under different ambient temperatures, we considered ambient temperature as a variable, keeping other parameters constant: rated current at 580A, wind speed at 1 m/s, wind direction angle at 90°, forced convection, solar irradiance at $S = 300\,\mathrm{W/m^2}$, and elevation at 2250m. Ambient temperatures (see fig. 7) from July 5 to July 7, 2022, were collected from Xining, a representative city in the high-altitude cold zone of China. As depicted in fig.7, the highest and lowest temperatures on July 5 were 25.73°C and 8.83°C, respectively; on July 6, they were 30.82°C and 10.43°C; and on July 7, they were 32.59°C and 12.75°C, with a range of 8.83°C to 32.59°C. Therefore, a temperature range of 10°C to 30°C was used to study the variations in the radial temperature and stress fields of overhead conductors with changes in ambient temperature.

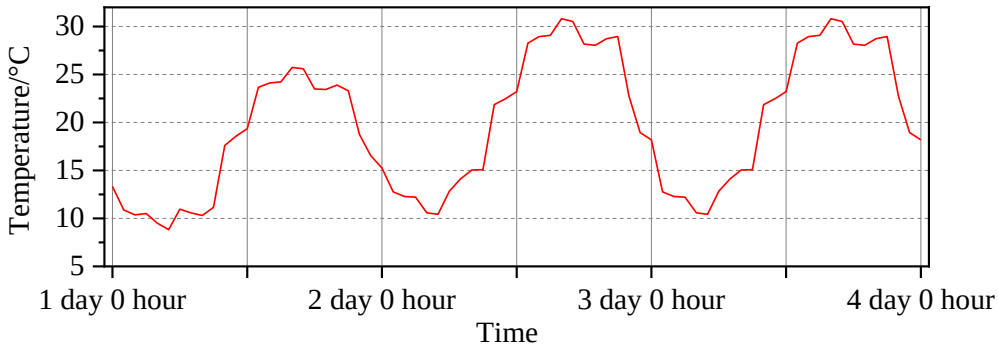

Figure 7. Ambient temperature from July 5th to 7th, 2022

Figure 10 shows the variations in the layered stresses of the overhead conductor with changes in ambient temperature. Its horizontal axis represents the number of layers of overhead wires, from inside to outside, numbered from 1, 2, 3, 4, 5, without units; The vertical axis denotes the layered stress, with unit in MPa. The legend in fig.10 is the ambient temperature, which is 10℃, 15℃, 20℃, 25℃, 30℃,respectively. From the data, it is observed that as the temperature increases from 10°C to 30°C, the stresses of the internal steel core (in the 1st and 2nd layers) increase from 52.981 MPa to 87.925 MPa (with a fluctuation of 34.944 MPa), and from 52.759 MPa to 87.508 MPa (with a fluctuation of 34.749 MPa), respectively. The stress in the external aluminum strands (in the 3rd, 4th, and 5th layers) changes from 6.111 to 9.063 MPa (with a fluctuation of 2.952 MPa), from 10.114 to 12.978 MPa (with a fluctuation of 2.864 MPa), and from 16.782 to 19.574 MPa (with a fluctuation of 2.792 MPa). This suggests that in the high-altitude cold zone, significant diurnal temperature variations can cause substantial fluctuations in conductor operating temperatures, leading to significant stress changes, thus impacting its performance.

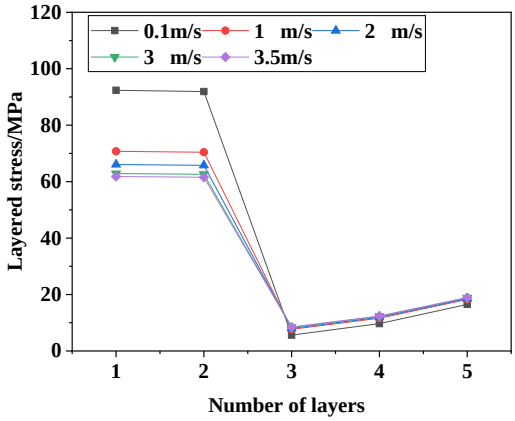

Figure 8. Variation of layered stresses with changes in wind speeds

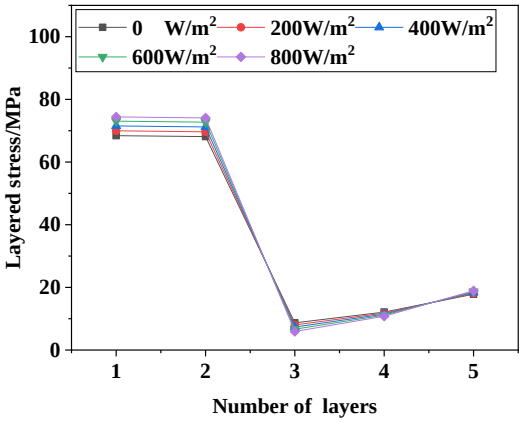

Figure 9. Variation of layered stresses with changes in solar irradiance

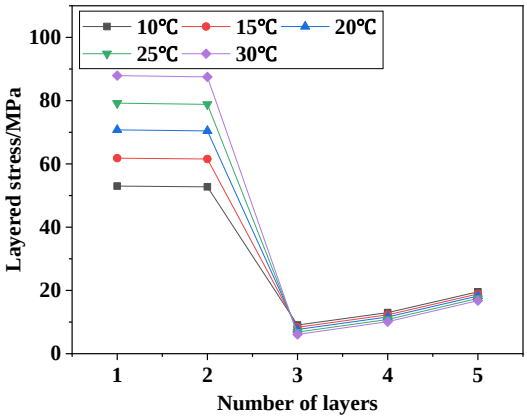

Figure 10. Variation of the layered stresses with changes in ambient temperature

4.2.4. Comparison of the three climate factors

Considering the impacts of three environmental factors on the layered stresses, it can be observed from the results in sections 4.2.1~4.2.3 that: when the wind speed increases from 0.1 m/s to 3.5 m/s, and the steel core stress decreases from 92.358 MPa to 61.807 MPa with a reduction of 30.551 MPa; when the solar irradiance increases from 0 to 848.036 W/m^2, and the steel core stress increases from 70.748 MPa to 74.973 MPa achieving an increase of 4.225 MPa; when the ambient temperature rises from 10°C to 30°C, and the steel core stress increases from 52.981 MPa to 87.925 MPa observing an increase of 34.944 MPa.

From the fluctuations in layered stress caused by these three factors, it is determined that within the study range of the high-altitude cold zone, the most significant factor affecting layered stresses is the ambient temperature, followed by wind speed, and lastly, the solar irradiance.

4.3. Analysis of the layered stresses in response to varying climatic conditions

Considering the effects of the three environmental factors (i.e., wind speed, solar irradiance, and ambient temperature) on the layered stresses, the time-histories of layered stresses of overhead conductors are calculated. The stress variations from the innermost to the outermost layers, from the 1st to the 5th layer, are shown in fig. 11. The trend observed in the figure indicates that: 1) The inner steel core, comprising the 1st and 2nd layers, exhibits a consistent stress trend, while the outer aluminum strands, consisted of the 3rd to 5th layers, display a similar trend; 2) The steel core's stress peaks occur at midday, with the lowest values at dawn, whereas the aluminum strands exhibit the opposite trend, with low values at midday and high values at dawn. Locally: 1) The highest and lowest internal stresses were observed at 8 PM on July 6th and at midnight on July 5th, respectively; 2) The fluctuations in the maximum stress (at 1st layer), minimum stress (at the 5^{th} layer) across the conductor's cross-section ranged from 46.191 to 104.953 MPa (showing a fluctuation amplitude of 58.762 MPa), and 3.978 to 10.49 MPa (with a fluctuation amplitude of 6.512 MPa), respectively. Due to the climate conditions in high-altitude cold zone, the overhead conductor stress field

exhibits significant fluctuations, with the maximum stress fluctuation reaching up to 58.762 MPa.

To further discuss the variation in the contributions of the aluminum strands and steel core to the longitudinal cross-sectional resistance of the overhead conductor under the changing climate conditions in high-altitude cold zone, fig. 12 presents the proportion of the steel core's resistance to that of the aluminum strands in three days. The figure reveals that: During the hot midday, the aluminum strands, due to thermal expansion, bear less tensile force, leaving the steel core to handle relatively great remaining tensile forces; Conversely, at the cold dawn temperatures, the reduced thermal expansion of the aluminum strands leads to an increased tensile force they bear, thus reducing the tensile force handled by the steel core. The resistance contribution ratio between the overhead conductor's steel core and aluminum strands reached its maximum and minimum values at 5 AM on July 5th and 8 PM on July 6th, respectively, indicated as 0.262 and 0.849 in the figure. It should be noted that in the Xining city, sunset occurs relatively late in the July, typically around 8:40 PM. In the operational environment of high-altitude cold zones, the resistance contribution ratio between the steel core and aluminum strands within overhead conductors exhibits significant fluctuations. For example, the resistance contribution ratio for the LGJ-400/35 conductors ranges from 0.262 to 0.849, achieving a fluctuation magnitude of 0.587.

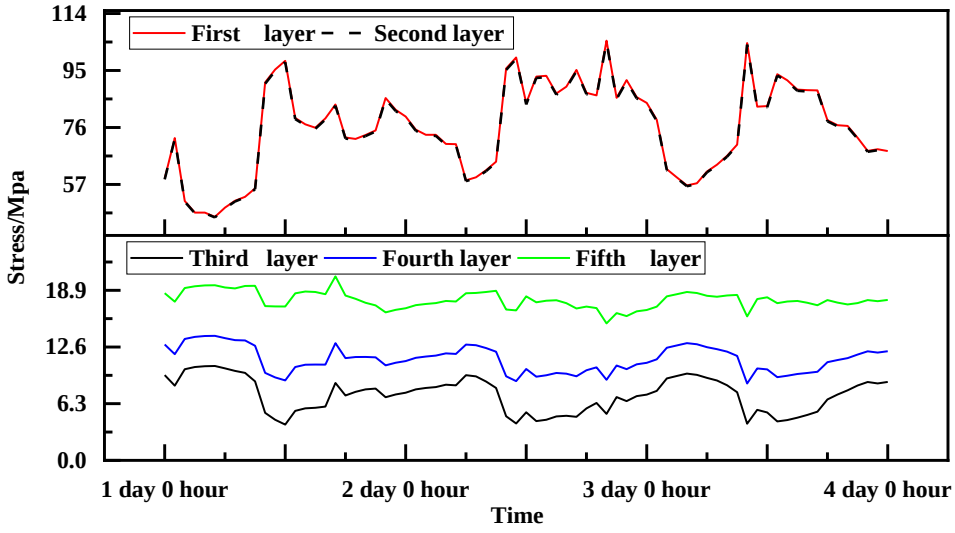

Figure 11. Time histories of the layered stresses in three days

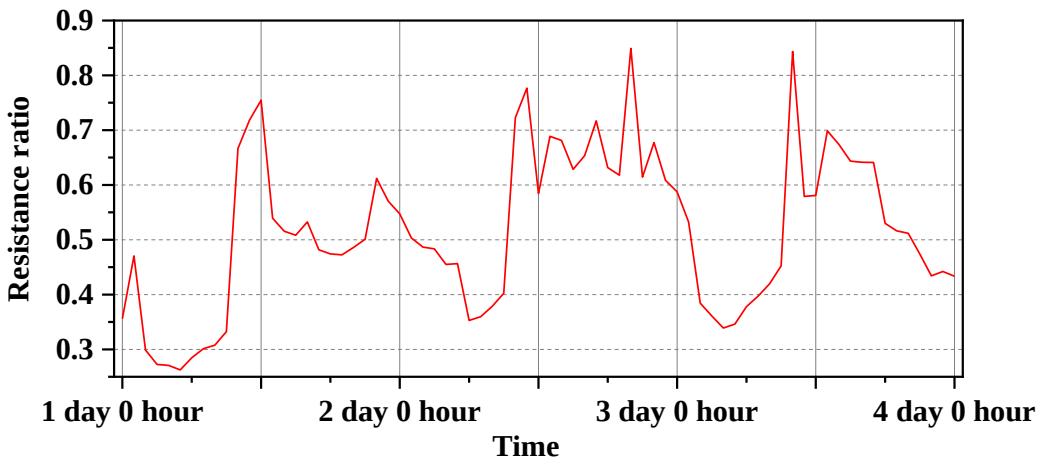

Figure 12. Proportion of the steel core's resistance to that of the aluminum strands

5. Conclusion

This study investigated the layered stress distribution of overhead conductors, as well as the variations in the layered stresses in response to changes in ambient temperature, wind speed, and solar irradiance. The analysis of the computational results under various conditions leads to the following conclusions:

a. Analysis of fluctuations in stress caused by single factors reveals that ambient temperature has the greatest impact on layered stresses, followed by wind speed, and finally solar irradiance.

b. Considering the three climatic conditions together, stresses in the steel core and the outermost aluminum wires vary in the range 46.191~104.953 MPa and 3.978~10.49 MPa, respectively. Such significant stress fluctuations are likely to cause fatigue and strand breakage issues in the overhead conductors.

c. As the conductor temperature increases, the proportion of stress borne by the external aluminum wires decreases, while the stress proportion in the internal steel core increases. The internal tensile force shifts from the aluminum strands to the steel core, causing the aluminum strands to progressively lose their load-bearing capacity.

6. Acknowledgement

The authors would like to acknowledge the financial support from the Qinghai Provincial Basic Research Program, project number 2023-ZJ-962Q. Any opinions, findings, conclusions, or recommendations expressed in this publication are those of the authors and do not necessarily reflect the views of the sponsors.

7. References

[1] Liu, G., *et al*., Effect of Radial Temperature Difference on Sag Calculation for Overhead Conductors (in Chinese), *Journal of South China University of Technology (Natural Science Edition), 45*(2017), 7, pp. 41-47+54.

[2] Wang, G., *et al*., Calculation of Stress and Sag of the Energy-Saving Capacity-Expanded Conductors (in Chinese), *Wire & Cable*,4(2009), 5, pp.11-14.

[3] Zhang, Y., Analysis and Calculation on Tensile Sag Characters of Double Capacity Conductor (in Chinese), *Electric Power Construction*, 27(2006), 9, pp. 7-9.

[4] Zainuddin, N. M., *et al*., Review of thermal stress and condition monitoring technologies for overhead transmission lines: Issues and challenges, *IEEE Access*, 2020, 8, pp. 120053-120081.

[5] Howington, B., *et al*., AC Resistance of ACSR - Magnetic and Temperature Effects Prepared by a Task Force of the Working Group on Calculation of Bare Overhead Conductor Temperatures, *IEEE Power Engineering Review*, 1985, 6, pp. 67-68.

[6] Foss, S. D., *et al*., Significance of the conductor radial temperature gradient within a dynamic line rating methodology, *IEEE transactions on power delivery*, 2(1987), 2, pp. 502-511.

[7] Douglass, D., Radial and axial temperate gradients in bare stranded conductor, I*EEE Transactions on Power Delivery*, 1(1986), 2, pp. 7-15.

[8] Morgan, V.T., Rating of bare overhead conductors for intermittent and cyclic currents, *Proceedings of the Institution of Electrical Engineers*, 116(1969),8, pp. 1361-1376.

[9] Morgan, V.T., Rating of bare overhead conductors for continuous currents, *Proceedings of the Institution of Electrical Engineers*, 114(1967),10, pp.1473-1482.

[10] Bena, L., *et al*., Calculation of the overhead transmission line conductor temperature in real operating conditions, *Electrical Engineering*, 2(2021), 103, pp. 769-780.

[11] Lin, J., *et al*., Research on Aluminum Conductor Steel Reinforced Tension Layered Characteristics of Overhead Conductors (in Chinese), *Wire & Cable*, 4(2015), 4, pp. 30-33.

[12] Li, P., et al., Section Stress Analysis of Overhead Conducting Wires (in Chinese), *Mechanical design and manufacturing*, 35(2020), 7, pp. 146-149+55.

[13] Morgan, V. T., Effect of elevated temperature operation on the tensile strength of overhead conductors, *IEEE Transactions on Power Delivery*, 11(1996), 1, pp. 345-352.

[14] Rawlins, C. B., Flexural self-damping in overhead electrical transmission conductors, *Journal of sound and vibration*, 323(2009), pp.232-256.

[15] He, Z., *et al*., ANSYS Calculation Method of Temperature and Current-carrying Capacity for Transmission Lines (in Chinese), *Zhejiang Electric Power*, 29(2010), 8, pp. 1-5.

[16] CIGRE., Thermal behavior of overhead conductors, *Electra*, 144(1992), pp.107-125.

[17] Liang, G., Finite Element Language and Its Applications (in Chinese), *Science Press*., Beijing, CHINA,2013.

[18] Liu, Y., *et al*., Numerical algorithms for calculating temperature, layered stress, and critical current of overhead conductors, *Mathematical Problems in Engineering*, (2020)2020, pp.1-14.

[19] IEEE Power Engineering Society., IEEE Standard for Calculating the Current-temperature Relationship of the bare overhead conductor, The Institute of Electrical and Electronics Engineers Inc., New York, USA, 2013.

[20] Cai, S., *et al*., Application of the Layer Characteristics to the Intensity of Overhead Conductors (in Chinese), *Southern Power System Technology*, 3(2009), pp.49-51.

[21] Cai, S., *et al*., Application and Study on Stratified Mechanical Model of Overhead Conductors (in Chinese), *Electric Power Construction*, 30(2009), 11, pp. 8-12.

[22] Zheng, L., *et al*., Stress Analysis of Aluminum Stranded Wire and Stee-l cored Aluminum Stranded Wire (in Chinese), *Engineering Journal of Wuhan University*, 1997, 3, pp. 66-69.

[23] Shao, T., Mechanical Calculation of Overhead Power Line Conductors, Electric Power Press (in Chinese)., Beijing, China, 2003.

[24] Xiao, K., *et al.*, Numerical Analysis on Temperature and Stress Filed Coupling of Overhead Conductors (in Chinese), *Guangdong Electric Power*, 28(2015), 11, pp. 97-102.

[25] General Administration of Quality Supervision Inspection and Quarantine, Standardization Administration of GB China., Round wire concentric lay overhead electrical stranded Conductors GB/T 1179—2017, Standards Press of China (in Chinese)., Beijing, CHINA, 2017.

Submitted: 14.7.2024.

Revised: 7.11.2024.

Accepted: 9.11. 2024.